Analytic bond-order potential for predicting structural trends across the *sp*-valent elements

Ralf Drautz,[1] Dewey A. Murdick,[2] Duc Nguyen-Manh,[3] Xiaowang Zhou,[2] Haydn N. G. Wadley,[2] and David G. Pettifor[1]
[1]*Department of Materials, The University of Oxford, Parks Road, OX1 3PH, Oxford, UK*
[2]*School of Engineering and Applied Science, University of Virgina, Charlottesville, VA 22904, USA*
[3]*UKAEA Fusion, Culham Science Centre, Abingdon, OX14 3DB, UK*
(Received 6 May 2005; published 17 October 2005)

An analytic interatomic bond-order potential (BOP) is derived that depends explicitly on the group number of the *sp*-valent element. This is achieved by generalizing the previously published BOP for group-IV elements by extrapolating from half-full occupancy using a simple envelope function for the upper bound of the bond order. This interatomic potential predicts the structural trends across the *sp*-valent elements that are found by our tight-binding reference calculations and observed by experiment. Unlike empirical interatomic potentials this theoretically derived BOP includes the valence-dependent character of the bonding naturally within its remit.

DOI: 10.1103/PhysRevB.72.144105 PACS number(s): 61.50.Ah, 61.66.Bi, 61.50.Lt

I. INTRODUCTION

The periodic table of the elements provides a stringent test bed for checking the range of applicability of different classes of interatomic potentials. For example, the embedded atom method[1] and Finnis-Sinclair[2] potentials have been found to model defect behavior reliably in close-packed metallic systems but not in bcc transition metals and their alloys.[3] Stillinger-Weber[4] and the more sophisticated environment-dependent interatomic potential[5] (EDIP) have performed robustly provided they are restricted to the group-IV elements C (Ref. 6) and Si.[7] Tersoff[8] and Brenner[9] reactive empirical bond-order (REBO) potentials have been applied successfully to hydrocarbons and group-IV elements, but have problems modeling the growth of III-V GaAs films where the description of As-rich surfaces is unphysical.[10] Recently, reactive force fields (ReaxFFs) have been developed for the hydrocarbons,[11] *sp*-valent elements, and transition metals,[12] but their analytic form is essentially empirical, requiring some 50 fitting parameters for each individual element and many more for multicomponent systems.

Empirical interatomic potentials, therefore, often lack transferability beyond a given narrow range of valence unless they are heavily parametrized with many fitting parameters that can lead to severe instabilities . This is due to their functional forms not embracing the intricacy of chemical bonding that is displayed within the periodic table. This is reflected, for example, in the structural trend across the *sp*-valent elements from the close-packed metals of groups I, II, and III through the open diamond structure of group IV, to the stacking of threefold-coordinated puckered layers in the group-V pnictides, the twofold-coordinated helical chains in the group-VI chalcogenides, and the singly coordinated dimers of the group-VII halogens.[13] This behavior across the non-close-packed systems is elegantly summed up by the well-known rule of chemistry that the local coordination z is given by $(8-N)$, where N is the valence or group number.

Twenty years ago Allan and Lannoo[14] showed that this structural trend across the *sp*-valent elements is predicted by a nearest-neighbor orthogonal tight-binding (TB) model, since it captures correctly the quantum mechanical nature of the chemical bond. Later Cressoni and Pettifor[15] focused directly on the very small differences in energy between one structure and the next by using the structural energy difference theorem.[16,17] This states that the difference in total energy between two structures in equilibrium is given solely by the difference in their attractive bond energies, once the bond lengths have been adjusted to give rise to the same repulsive energy per atom. This allowed the structural trends to be interpreted directly in terms of the topology of the local atomic environment through the behaviour of the first few moments of the electronic densities of states (DOS). In particular, following the connection between the pth moment of a TB DOS and self-returning hopping or bonding paths of length p within the lattice,[18] they showed that the third moment was responsible for the close-packed to open behavior across a period, reflecting the presence of three-membered rings in the former structures and their absence in the latter. On the other hand, they found that the fourth moment, which measured the bimodality of the DOS, drove the structural trends reflected in the $(8-N)$ rule for open structures.

This direct link between structural stability, valence, and hopping paths of a particular length within the lattice has been rendered explicit by bond-order potential (BOP) theory.[19–21] This leads to an exact many-atom expansion for the bond order in terms of a sum over one-hop, two-hop, three-hop, etc., interference paths that link the atoms at the two ends of the bond.[22] Importantly each contribution has its own prefactor that depends not only on the moments of the local DOS, but also on the valence. This so-called *numerical* BOP formalism has been applied successfully to modeling grain boundaries and dislocations by taking the many-atom expansion to convergence and using Hellmann-Feynman forces within static relaxation.[23–25] Recently, in order to perform molecular dynamics simulations, the convergence of the BOP expansion has been improved by imposing a constraint on the poles of the intersite Green's function that determines the bond order.[26] This allowed the derivation of *analytic* BOPs, which have been published for the case of half-full *sp*-valence shells.[27,28] They are currently being ap-

plied to modeling the growth of Si and GaAs films using analytic forces within molecular dynamics.[29,30]

In this paper we will introduce a simple extrapolation scheme that allows us to extend these analytic BOPs to any valence or band filling within *sp*-bonded systems. We will then demonstrate that these potentials predict the structural trends across the periodic table which we have mentioned above. We begin in Sec. II by discussing the structural trends and corresponding structure maps that are computed within the reduced TB approximation[31,32] that underpins analytic BOP theory. In Sec. III the framework of analytic BOPs will be briefly outlined and an important upper bound on the magnitude of the bond order is derived. In Sec. IV we generalize our previous analytic BOP expressions for half-full valence shells to any valence or band filling. In Sec. V we compare the structural trends and structure maps predicted by these analytic BOPs with those computed by **k**-space TB in Sec. II. In Sec. VI we conclude.

II. *sp*-VALENT STRUCTURE MAPS WITHIN TIGHT BINDING

A. The reduced TB model

In this section we present the reduced TB model that underpins the analytic BOPs and define the relevant physical parameters that will enter the final expression for the σ and π bond orders. In 1991, Cressoni and Pettifor[15] demonstrated that the structural trends across the periodic table could be understood within an orthogonal nearest-neighbor TB model in which the binding energy per atom U takes the simple form

$$U = U_{\mathrm{rep}} + U_{\mathrm{bond}}. \tag{1}$$

The first term arises from the overlap repulsion and is assumed to be pairwise, so that

$$U_{\mathrm{rep}} = \frac{1}{2N_{\mathrm{at}}} \sum_{i \neq j} \Phi(R_{ij}), \tag{2}$$

where R_{ij} is the distance between neighbors i and j and N_{at} is the number of atoms in the system. The second term is the attractive covalent bond energy

$$U_{\mathrm{bond}} = \frac{1}{N_{\mathrm{at}}} \sum_{\alpha=s,p} \int^{\epsilon_F} (\epsilon - \epsilon_\alpha) n_\alpha(\epsilon) d\epsilon, \tag{3}$$

where $n_{s(p)}$ are the local s (p) electron densities of states, $\epsilon_{s(p)}$ are the on-site s (p) atomic energy levels, and ϵ_F is the Fermi energy. In this paper we will neglect the *s*-*p* atomic energy level splitting and take $\epsilon_p = \epsilon_s$. Cressoni and Pettifor[15] considered the general case $\epsilon_p \neq \epsilon_s$ and included the corresponding promotion energy in Eq. (1). However, they found that the structural trends within the *sp*-valent elements were well represented by the simplest case $\epsilon_p = \epsilon_s$, apart from the appearance of the anomalous fcc structure of Pb in Group IV which they argued was driven by the large *sp* splitting arising from relativistic effects.

The bond energy Eq. (3) may be decomposed in terms of the contributions from the individual bonds, namely,

$$U_{\mathrm{bond}} = \frac{1}{2N_{\mathrm{at}}} \sum_{i \neq j} U_{\mathrm{bond},ij}, \tag{4}$$

where

$$U_{\mathrm{bond},ij} = 2 \sum_{m,m'} H_{im,jm'} \Theta_{jm',im}. \tag{5}$$

The Hamiltonian and bond-order matrix elements are given with respect to the valence orbitals $|im\rangle$ and $|jm'\rangle$ on sites i and j, respectively. The former matrix elements are evaluated within the usual Slater-Koster two-center approximation.[33] The matrix product on the right-hand side of Eq. (5) may be further simplified by making the reduced TB approximation[31,32] in which the $sp\sigma$ bond integral is replaced by the geometric mean of $|ss\sigma|$ and $pp\sigma$. This approximation is valid to within 16% for Harrison's canonical TB parametrization[34] and to within 12% for Xu *et al.*'s parametrization of carbon.[35]

The individual bond energies now take the chemically intuitive form

$$U_{\mathrm{bond},ij} = 2\beta_\sigma(R_{ij}) \Theta_{\sigma,ij} + 2\beta_\pi(R_{ij}) (\Theta_{\pi_+} + \Theta_{\pi_-})_{ij}, \tag{6}$$

where the σ bond is characterized by the single (scalar) bond order Θ_σ and the π bond is characterized by the two bond orders Θ_{π_+} and Θ_{π_-}. The two fundamental bond integrals are negative quantities whose magnitudes are given by

$$|\beta_\sigma| = |ss\sigma| + pp\sigma,$$

$$|\beta_\pi| = |pp\pi|. \tag{7}$$

Within this reduced TB approximation the three independent Slater-Koster σ bond integrals $ss\sigma$, $pp\sigma$, and $sp\sigma$ have been reduced to two independent parameters, namely, β_σ and p_σ, where

$$p_\sigma = \frac{pp\sigma}{|ss\sigma| + pp\sigma}. \tag{8}$$

We see that p_σ takes values in the range $0 \leqslant p_\sigma \leqslant 1$ and determines the relative amount of s and p admixture in the bonding hybrid orbital.[31,32] For $p_\sigma = 0$ only s orbitals contribute to the σ bond, whereas for $p_\sigma = 1$ the bond has pure p character.

In this paper we also define a parameter p_π to measure the relative strength of the π and σ bond integrals, namely,

$$p_\pi = \beta_\pi / \beta_\sigma. \tag{9}$$

We assume that β_σ and β_π display the same distance dependence so that p_π is a constant, independent of bond length. Finally, following Goodwin, Skinner, and Pettifor,[36] we assume that the distance dependence of the repulsive pair potential is related to that of the bond integrals through

$$\Phi(R) \propto \beta_\sigma(R)^\lambda. \tag{10}$$

λ is a measure of the hardness of the repulsive potential, which is totally soft for $\lambda = 1$ but totally hard for $\lambda = \infty$.[17] It is expected that $\lambda \approx 2$ for the case of repulsion arising from second-order overlap contributions. This is borne out by den-

sity functional theory calculations on *sp*-valent dimers where λ equals 1.6 and 1.9 for C and Si, respectively.[30]

B. Reduced TB structure maps

In this section we compare the relative stability of different simple structures of *sp*-valent elements as a function of the number of valence electrons N within the reduced TB model. The resultant structural trend across the periodic table reflects the change in bonding character with valence that we would like our analytic BOPs to include explicity. We consider, in particular, nearest-neighbor structure types with coordinations ranging from $z=1$ (dimer), $z=2$ (a helical chain with 90° bond angles), $z=2'$ (a linear chain), $z=3$ (a puckered graphene sheet with 90° bond angles), $z=3'$ (a planar graphene sheet), $z=4$ (diamond), $z=6$ (simple cubic), $z=8$ (ideal simple hexagonal), and $z=12$ (fcc). We have not included hcp among the structures, because our analytic BOP cannot differentiate between fcc and hcp since it does not include explicitly the fifth- and sixth-moment contributions that drive the extremely small energy difference between cubic and hexagonal close packed.[15] We have used the Jensen notation[37] $2'$ and 2, $3'$ and 3 to distinguish between the twofold-coordinated linear and helical chains, and the threefold-coordinated planar and puckered graphene sheets, respectively.

The relative stability of the different structure types is evaluated using the structural energy difference theorem.[16,17] This states that the difference in total energy between two structures ΔU in equilibrium is given to first order by the difference in their bond energies provided that the bond lengths have been adjusted to give rise to the same repulsive energy per atom, i.e.,

$$\Delta U^{(1)} = (\Delta U_{\mathrm{bond}})_{\Delta U_{\mathrm{rep}}=0}. \tag{11}$$

This theorem can be understood from a physical point of view for the particular case where the repulsive potential falls off as the square of the bond integrals, corresponding to $\lambda=2$ in Eq. (10). In this case an identical repulsive energy in the two structures corresponds to an identical second moment μ_2 of the density of states, or in other words the same root mean square width of the two eigenspectra. This follows mathematically from

$$\Delta\mu_2 = 0 \Leftrightarrow \Delta\{z[\beta_\sigma^2(R_z) + 2\beta_\pi^2(R_z)]\} = 0$$

$$\Leftrightarrow \Delta[z\Phi(R_z)] = 0 \Leftrightarrow \Delta U_{\mathrm{rep}} = 0, \tag{12}$$

where R_z is the corresponding bond length for the structure with coordination z. The first implication results from the theorem by Cyrot-Lackmann[18] which relates the pth moment of a TB density of states to the sum over all self-returning paths of length p within the structure. The second implication is a consequence of the distance dependence of the repulsive pair potential in Eq. (10).

The importance of this theorem is that it breaks down the evaluation of the structural energy difference into two well-defined steps. In the first step the bond lengths are adjusted until all the structures display the same repulsive energy per atom, which from Eq. (10) corresponds to scaling the TB bond integrals as

$$\beta_\sigma(R_z) = \beta_0/z^{(1/\lambda)}, \tag{13}$$

where β_0 is the σ bond integral for the dimer. In the second step the eigenstates are filled with electrons and the bond energies of the different structures are compared to identify the most stable structure as a function of the number of valence electrons N. This avoids the tedious procedure of first computing the equilibrium bond lengths for all the individual structure types corresponding to a given single-electron occupancy N and then finding the resultant differences in the total binding energies. But most significantly the structural energy difference theorem separates out the role of the hardness of the repulsive potential (through λ) from the quantum mechanical bonding properties of the valence electrons (through the behavior of the bond orders Θ_σ and Θ_π as a function of N).[17] The customary approach of working directly with the total binding energy curves disguises these individual contributions from repulsion and bonding.

It follows from Eqs. (5) and (12) that within the reduced TB approximation the bond energy per atom of these simple first-nearest-neighbor-coordinated structures can be written in the form

$$U_{\mathrm{bond}} = -z^{(1-1/\lambda)}\{\Theta_\sigma^z(p_\sigma,p_\pi,N) + p_\pi[\Theta_{\pi+}^z(p_\sigma,p_\pi,N) + \Theta_{\pi-}^z(p_\sigma,p_\pi,N)]\}|\beta_0|. \tag{14}$$

We see that whereas the energy scale is set by the magnitude of the σ bond integral $|\beta_0|$ for the dimer, the bond orders themselves depend only on the two reduced TB parameters p_σ and p_π, which determine the amount of p admixture in the σ hybrid and the relative strength of the π to σ bond integral, respectively. In addition, the influence of λ, which reflects the hardness of the repulsive potential,[17] enters only through a single coordination-dependent prefactor. For $\lambda=2$, this prefactor varies as the square root of the coordination, as expected from the linear dependence of the bond energy on the bandwidth which scales as the square root of the second moment [cf. Eq. (12)].

Thus, for a given number of valence electrons N, the relative stability of these different structures is controlled by the three parameters p_σ, p_π, and λ. Figure 1 shows the resultant structure maps (p_σ,N) for three different choices of $p_\pi/p_\sigma(p_\pi/p_\sigma=0,1/4,1/2)$ and λ (λ=1.8, 2.0, 2.2). They were obtained by computing the TB bond orders that enter Eq. (14) using the **k**-space routine within the OXON package.[38] Let us concentrate first on the central structure map corresponding to Harrison's canonical TB value[34] of $p_\pi/p_\sigma=1/4$ and hardness coefficient $\lambda=2.0$. We see that if we proceed along the horizontal dashed line for $p_\sigma=2/3$ (Harrison's canonical TB value[34]), then we proceed from the dark blue domain of close-packed stability around groups I and II to the narrow purple domain of simple hexagonal stability around group III, to the green domain of diamond stability around group IV, to the yellow-orange and red-orange domains of three fold-coordinated graphene and puckered graphene sheets around group V, to the yellow do-

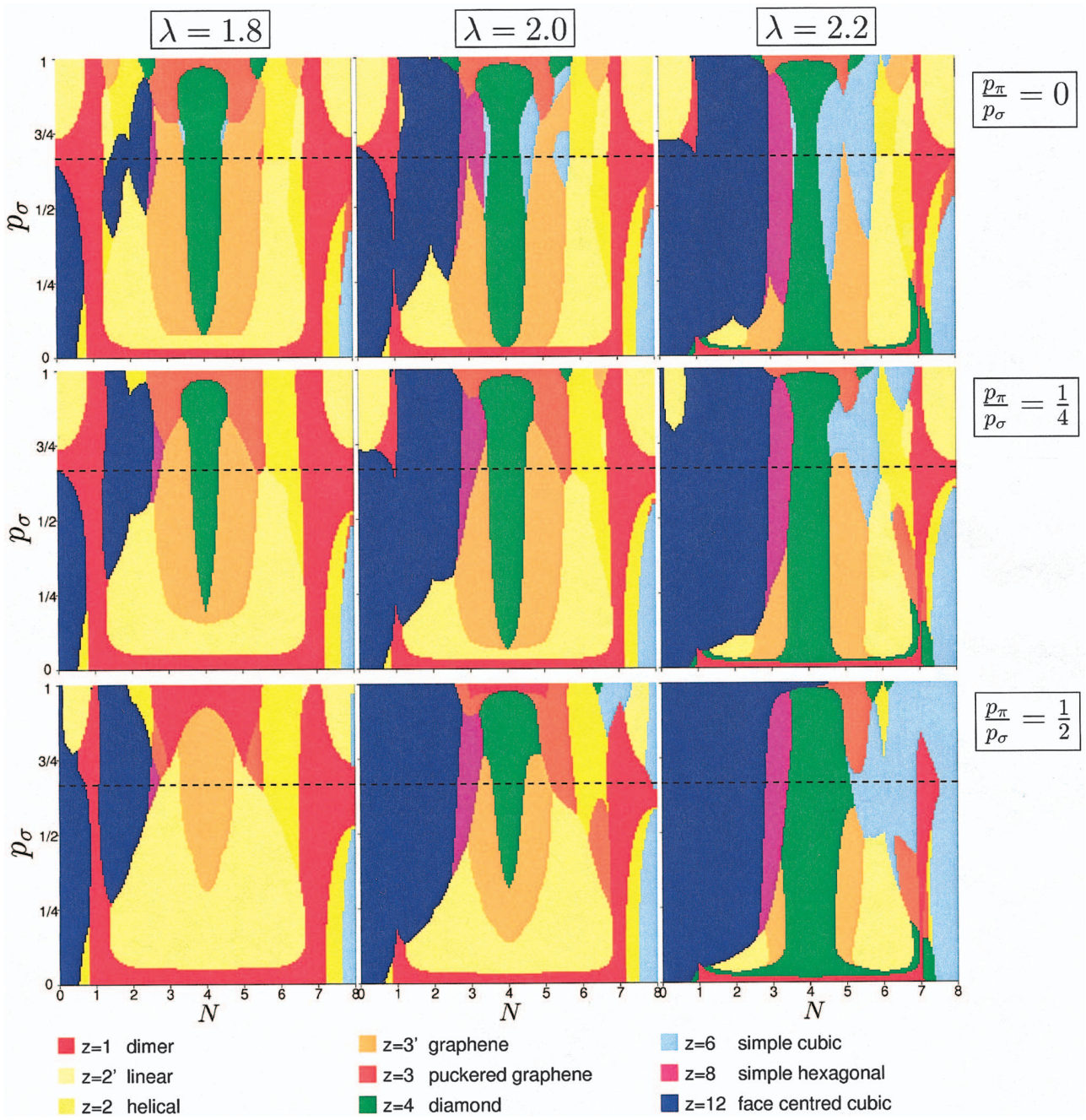

FIG. 1. (Color) The most stable structure as a function of the bonding parameters p_σ, p_π and the exponent of repulsion λ for a given number of valence electrons N. The black dashed lines correspond to Harrison's canonical value of $p_\sigma=2/3$ (Ref. 34).

main of two fold-coordinated helical chains around group VI, and finally to the red domain of the singly coordinated dimers around group VII.

This trend with $p_\sigma=2/3$, $p_\pi=1/6$, $\lambda=2.0$ agrees well with the observed structural trends across the *sp*-valent elements which we discussed in the introductionary section, apart from the eightfold-coordinated simple hexagonal stability around group III. We find that this trend remains broadly unchanged if the π bonding is either turned off (as in the top central map) or increased by a factor of 2 (as in the bottom central map). This is consistent with the well-known fact that the $z=(8-N)$ rule is driven by the saturated σ bonds within the open structures.[17]

On the other hand, the observed deviations from the $(8-N)$ rule can be accounted for by the variation in the hardness of the repulsive potential through the parameter λ. The first-row $2p$-valent elements have softer cores than their counterparts in the remaining rows due to the absence of p electrons in their cores leading to much weaker overlap repulsion.[17] We see that reducing λ to 1.8 in the left-hand column of Fig. 1 results in the lower-coordination structures becoming more stable with respect to higher-coordinated structures. In fact, we observe that in the bottom structure map corresponding to $p_\pi/p_\sigma=1/2$ graphite has become the most stable structure for group IV if $p_\sigma<7/8$, whereas the dimer has become the most stable for group V if $p_\sigma>3/4$,

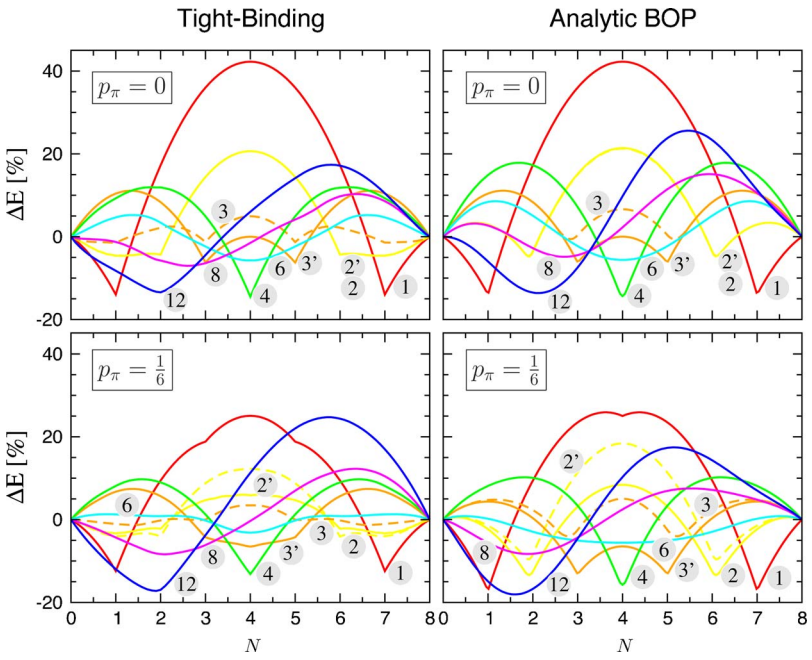

FIG. 2. (Color online) Comparison of the structural energies of reduced TB (in the left column) and analytic BOP (in the right column). The energies have been normalized with respect to the energy of a half-full rectangular band model with identical second moment. The upper and lower panels correspond to $p_\sigma=2/3$, $p_\pi=0$ and $p_\sigma=2/3$, $p_\pi=1/6$, respectively. Shown are the dimer (1), the linear chain (2′), the helical chain (2, dashed line), the graphene sheet (3′), the puckered graphene sheet (3, dashed line), cubic diamond (4), simple cubic (6), simple hexagonal (8), and face-centered cubic (12). For $p_\pi=0$ the linear chain (2′) and the helical chain (2) are degenerate. The values of the fitting parameter c_σ are 1.18 and 1.27 in the upper and lower right panels, respectively; c_π takes the value of 1 in both cases.

which is consistent with the "anomalous" ground-state structures of $2p$-valent C and N.

Cressoni and Pettifor[15] explained these trends for $\lambda=2$ by analyzing the behavior of their structural energy curves as a function of electron occupancy N. They defined the *structural energy* as the difference between the bond energy for a given structure and that corresponding to a reference rectangular DOS with the same second moment μ_2 as that implied by the structural energy difference theorem [cf. Eq. (12)]. The left-hand column of Fig. 2 shows the resultant structural energies for our reduced TB calculations with $p_\sigma=2/3$ and $p_\pi=0$ (upper panel) or 1/6 (lower panel). These curves have been normalized by the magnitude of the corresponding bond energy of the rectangular DOS for $N=4$, in order to emphasize the very small percentage differences in energy between one competing structure type and another. In particular, we can now understand why the group-III elements B, Al, and Ga display the very different structure types of eightfold-coordinated rhombohedral boron, 12-fold-coordinated fcc and sevenfold-coordinated α-Ga, respectively, since the eightfold simple hexagonal and the 12-fold-coordinated fcc curves intersect near $N=3$. The lower panel in Fig. 2 resulting from the reduced TB approximation with $p_\sigma=2/3$ and $p_\pi=1/6$ is very similar to that of Cressoni and Pettifor,[15] whose curves had been computed using Eq. (3) with the on-site DOS evaluated within the conventional Slater-Koster TB model.

The behavior of the structural energy curves in Fig. 2 can be rationalized in terms of the lowest few moments of the DOS, following the pioneering work of Cyrot-Lackmann[18] and Ducastelle and Cyrot-Lackmann.[39] In particular, the fact that the fcc and simple hexagonal curves are skewed and display one node as a function of band filling N implies that the third moment μ_3 is dominant, whereas the fact that the curves for the open structures are symmetric about half filling and display two nodes implies that the fourth moment μ_4 is dominant.[39] Thus the change from close-packed to open structures as the valence shell is filled with electrons is driven by the presence of three-member rings in the former and their absence in the latter. The structural competition between the open structures, on the other hand, is driven by the fourth moment, since all the structures have the same second moment μ_2 by the structural energy difference theorem and the same vanishing third moment μ_3. Cressoni and Pettifor[15] found that the structural trend from $z=4$ to $z=3$ to $z=2$ to $z=1$ on going from group IV to group VII indeed corresponds to the direction of increasing fourth moment. Diamond is the most stable structure for a half-full band since it has the lowest fourth moment and hence most bimodal DOS, whereas the dimer has the largest fourth moment which favors nearly full (or nearly empty) occupancies of the valence shell.[17,40] As mentioned in the Introduction, this link between the structural stability, electron occupancy and the moments of the local DOS has since been made formally explicit by BOP theory.[19–21]

III. ANALYTIC BOND-ORDER POTENTIALS

The framework of the analytic BOPs has been presented in detail in several papers[19,26–28,32,41] with a clear introduction being published by Finnis in Sec. 7.12 of his recent book.[42] In this section we, therefore, give only a short summary of the details we require for extending the formalism to arbitrary electron occupancy and derive important bounds to the bond order.

A. A bound to the bond order

The bond order that enters Eq. (5) for the individual bond energy is simply twice the well-known density matrix $\rho_{im,jm'}$, i.e.,

$$\Theta_{im,jm'} = 2\,\rho_{im,jm'} \quad (i \neq j). \tag{15}$$

The density matrix is defined from the expansion coefficients $c_{im}^{(n)}$ of the eigenstates $|\psi_n\rangle=\Sigma_{im}c_{im}^{(n)}|\phi_{im}\rangle$ in terms of the local,

real-valued basis functions $|\phi_{im}\rangle$. The density-matrix element linking the orbital m on site i to the orbital m' on site j is then obtained by summing over the occupied states,

$$\rho_{im,jm'} = \sum_{n(\mathrm{occ})} \langle \phi_{im}|\psi_n\rangle\langle\psi_n|\phi_{jm'}\rangle = \sum_{n(\mathrm{occ})} c_{im}^{(n)} c_{jm'}^{(n)}. \quad (16)$$

It is easily verified that Eqs. (4) and (5) follow by explicitly decomposing the band energy $\Sigma_{n(\mathrm{occ})}\langle\psi_n|\hat{H}|\psi_n\rangle$ in terms of the local basis functions.

The term "bond order" was introduced by the chemists[43] because the bond order is one-half the difference between the number of electrons in the bonding state compared to the antibonding state. That is,

$$\Theta_{im,jm'} = \frac{1}{2}(N_+ - N_-), \quad (17)$$

where $N_{+(-)}$ gives the number of electrons in the bonding (antibonding) state $|\pm\rangle = (|\phi_{im}\rangle \pm |\phi_{jm'}\rangle)/\sqrt{2}$. This follows from Eq. (16) since $2c_ic_j = \frac{1}{2}[(c_i+c_j)^2 - (c_i-c_j)^2]$. Thus, the hydrogen dimer with two electrons in the bonding state but none in the antibonding state corresponds to a saturated bond with $\Theta = 1$.

The purpose of analytic BOP theory is to derive explicit expressions for the dependence of the σ and π bond orders on the local atomic environment. In order to achieve this for a general electron occupancy, we need to prove that the magnitude of the bond order is bounded by the constraint

$$|\Theta_{im,jm'}| \leqslant \begin{cases} N_{im,jm'} & \text{for } 0 \leqslant N_{im,jm'} \leqslant 1, \\ 2 - N_{im,jm'} & \text{for } 1 < N_{im,jm'} \leqslant 2, \end{cases} \quad (18)$$

where $N_{im,jm'} = \frac{1}{2}(N_+ + N_-) = \frac{1}{2}(N_{im} + N_{jm'})$ is the number of electrons *per atom* associated with the bond between the orbitals m and m' on atoms i and j, respectively. The proof follows directly from Eq. (17) which can be written either as

$$\Theta_{ij} = \frac{1}{2}(N_+ - N_-) = N_{ij} - N_- \leqslant N_{ij} \quad (19)$$

or as

$$\Theta_{ij} = \frac{1}{2}(N_+ - N_-) = N_+ - N_{ij} \leqslant 2 - N_{ij}, \quad (20)$$

because $0 \leqslant N_{+(-)} \leqslant 2$, where $i \equiv im$, $j \equiv jm'$ in the subscripts above. Equations (19) and (20) are the two upper bounds for $0 \leqslant N_{ij} \leqslant 1$ and $1 \leqslant N_{ij} \leqslant 2$, respectively. The lower bounds are obtained from

$$\Theta_{ij} = \frac{1}{2}(N_+ - N_-) = N_+ - N_{ij} \geqslant -N_{ij}, \quad (21)$$

$$\Theta_{ij} = \frac{1}{2}(N_+ - N_-) = N_{ij} - N_- \geqslant N_{ij} - 2. \quad (22)$$

This proves Eq. (18).

The left-hand panel of Fig. 3 shows the dependence of the σ and π bond orders on the fractional occupancy f of the bond for different structure types. They were calculated for the particular case $p_\sigma = 2/3$, $p_\pi = 1/6$ using the **k**-space routine within the OXON package.[38] We see that the bond orders do indeed satisfy the bound constraints of Eq. (18), the right-hand side providing a simple linear envelope function for the regions $0 \leqslant f \leqslant 1/2$ and $1/2 \leqslant f \leqslant 1$, respectively. We will use this envelope function as a boundary condition in Sec. IV for extrapolating the analytic bond-order expression for half-full occupancy to any required fractional occupancy f.

B. Analytic bond orders for half-full occupancy

An analytic expression for the σ bond order of an *sp*-valent system with a symmetric DOS has been derived by truncating the Lanczos chain after four sites and using the constraint that the resultant four poles of the intersite Green's function G_{ij} must be the same as the poles of the average on-site Green's function $\frac{1}{2}(G_{ii}+G_{jj})$.[26–28] The σ bond order for the fractional occupancy $f = 1/2$ corresponding to filling the lowest two poles takes the compact form

$$\Theta_{ij,\sigma}^{(1/2)} = 1/\sqrt{1 + c_\sigma \frac{2\Phi_{2\sigma} + \Re_{4\sigma}^{(ij)} + \tilde{\Phi}_{2\sigma}^{(i)}\tilde{\Phi}_{2\sigma}^{(j)}(2 + \widetilde{\Delta\Phi}_{4\sigma})}{(1 + \widetilde{\Delta\Phi}_{4\sigma})^2}}, \quad (23)$$

where explicit formulas have been given in Refs. 27,28 for the *self-returning* two- and four-hop contributions and the three-hop *interference* contribution linking the two ends of the bonds i and j, corresponding to the four-member ring term $\Re_{4\sigma}^{(ij)}$. In this paper we have introduced a fitting parameter c_σ which takes the value 1 within this four-site approximation, but here it is allowed to take a constant value close to 1 in order to account for our neglect of higher-order hopping paths. In this work we calculated c_σ by matching the σ bond order of the simple cubic structure from analytic BOP to the reduced TB value at $p_\sigma = 2/3$, $p_\pi = 0$ ($c_\sigma = 1.18$) and $p_\sigma = 2/3$, $p_\pi = 1/6$ ($c_\sigma = 1.27$).

Analytic expressions for the π bond orders have been obtained[26] using the matrix form of the Lanczos algorithm,[44,45] in order to treat the p_x and p_y orbitals on an equal footing, thereby guaranteeing that the resultant π bond orders are independent of the choice of axes. Truncating the Lanczos chain after two sites leads to two uncoupled sets of poles, corresponding to π_+ and π_-. The $\pi_{+(-)}$ bond order for the fractional occupancy $f = 1/2$ then takes the compact form

$$\Theta_{ij,\pi_\pm}^{(1/2)} = 1/\sqrt{1 + c_\pi(\Phi_{2\pi} \mp \sqrt{\Phi_{4\pi}})}, \quad (24)$$

where explicit formulas have been given in Ref. 32 for the two- and four-hop contributions. Again a fitting parameter c_π has been introduced that should take a value close to 1, the value predicted within this second-moment matrix approximation. In this work we choose $c_\pi = 1$.

The beauty of these analytic expressions is that they automatically satisfy the constraint $\Theta \leqslant 1$ for half-full bands in Eq. (18). This is illustrated in Fig. 4 which compares the analytic and reduced TB σ and π bond orders as a function of the coordination z for $p_\sigma = 2/3$, $p_\pi = 1/6$ and $c_\sigma = c_\pi = 1$. We see that the analytic σ bond orders for the open structures reproduce accurately the TB values, but that larger errors arise for the more close-packed structures where the presence

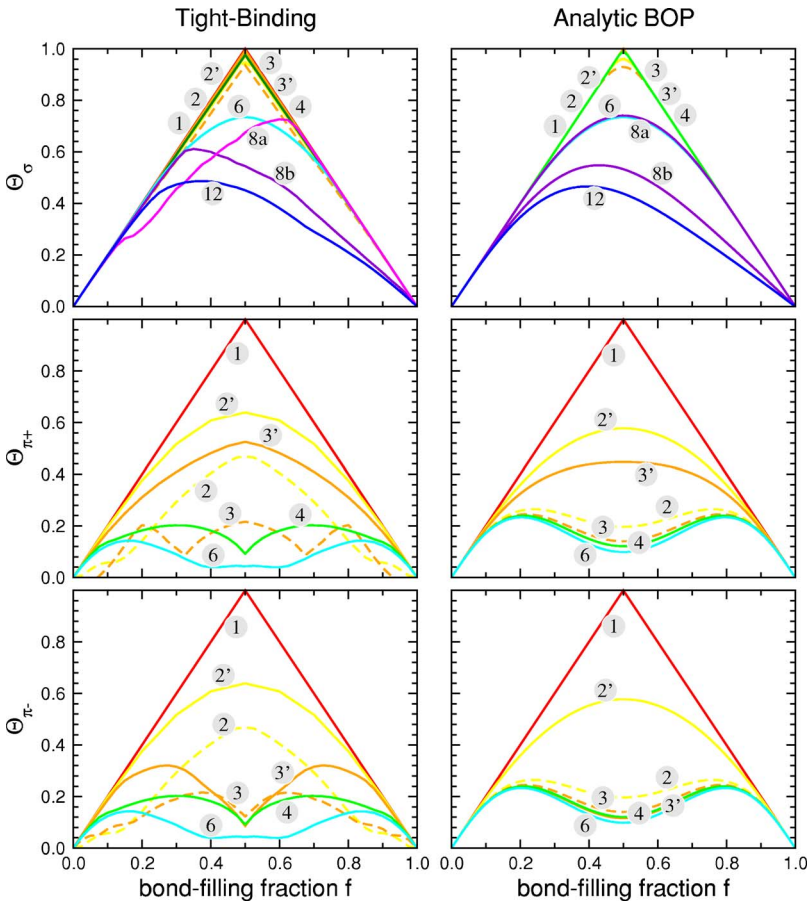

FIG. 3. (Color online) Bond order of the σ, π_+, and π_- bonds as a function of the fractional bond occupancy for the case $p_\sigma=2/3$, $p_\pi=1/6$. Shown are the dimer (1), the linear chain (2′), the helical chain (2, dashed line), the graphene sheet (3′), the puckered graphene sheet (3, dashed line), cubic diamond (4), simple cubic (6), simple hexagonal (8a and 8b for the axial and basal bonds, respectively), and face-centered cubic (12). For the π bonds only the structures with coordination $z\leqslant 6$ are shown. The BOP results were evaluated using the extrapolation scheme described in Sec. IV with $c_\sigma=1.27$ and $c_\pi=1$.

of the neglected three-membered rings causes the DOS to be nonsymmetric. We also see that the analytic π bond orders predict the large bifurcation between the saturated π_+ and the unsaturated π_- bonds that occurs in planar structures such as graphite. However, at the level of the second moment matrix approximation, the TB bifurcation of the fcc π bond orders into (0.05, −0.02) is not observed with the analytic BOP values remaining degenerate (0.07, 0.07). This error is not serious because both p_π and the magnitude of the π bond orders are small.

Finally, the importance of the four-hop and four-member ring contributions in Eqs. (23) and (24) can be judged by considering the results for only the two-hop contributions,[46] namely,

$$\Theta_{ij,\sigma(\pi)}^{(1/2)} = 1/\sqrt{1+\Phi_{2\sigma(\pi)}}, \tag{25}$$

where we have taken $c_\sigma=c_\pi=1$. For the special case of the first-nearest-neighbor structure types considered in this paper (but not including the helical chain, the puckered graphene layer and the simple hexagonal lattice), the analytic expressions reduce to the particularly simple forms for the σ bond[26,47]

$$\Theta_\sigma^{(1/2)}(2\text{hop}) = 1/\sqrt{z\left((1-p_\sigma)^2+\frac{1}{d}p_\sigma^2\right)}, \tag{26}$$

and for the π bond, generalizing Eq. (53) of Ref. 32 to general dimension d,

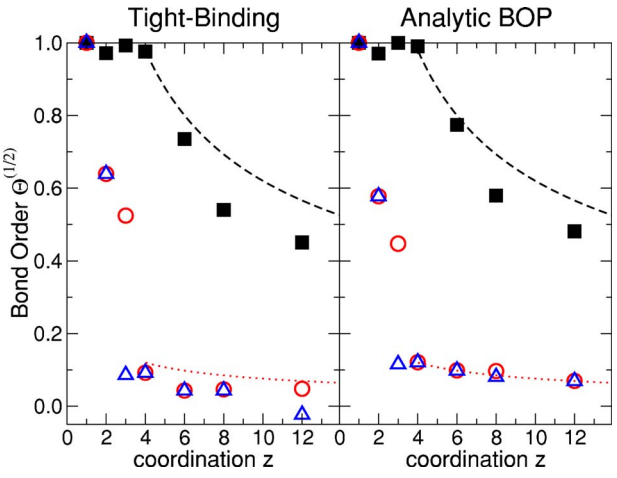

FIG. 4. (Color online) Reduced TB and analytic BOP σ bond order Θ_σ (■), π_+ bond order Θ_{π_+} (◯), and π_- bond order Θ_{π_-} (△) as a function of coordination z for a half-full band with $p_\sigma=2/3$ and $p_\pi=1/6$. For clarity we have plotted only the values for the linear chain (2′) and graphene sheet (3′) for two- and threefold coordination, respectively. All the first-nearest-neighbor bonds are equivalent in these structures apart from the eightfold-coordinated simple hexagonal structure, where we have presented the weighted average of the six basal and two axial bonds. The dashed and dotted lines correspond to the σ and π bond order, respectively, within the simplified two-hop approximation of Eq. (28). The BOP values were calculated with $c_\sigma=c_\pi=1$.

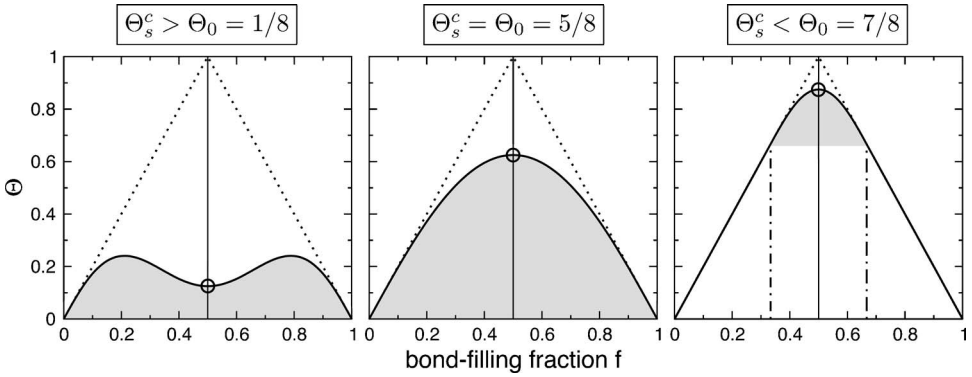

FIG. 5. Illustration of the extrapolation of the bond order for a symmetric eigenspectrum. The bond order at half-full band is shown by circles and takes the values $\Theta_0=1/8$, 5/8, and 7/8 in the left, central, and right panels, respectively. The envelope function of the bond order is indicated by dotted lines. In the right-hand panel the dot-dashed vertical lines correspond to $f_0=1/3$ and $(1-f_0)=2/3$, respectively.

$$\Theta_{\pi_+}^{(1/2)}(2\text{hop}) = \Theta_{\pi_-}^{(1/2)}(2\text{hop}) = 1/\sqrt{z\left[\left(1+\frac{1}{d}\right)+\left(1-\frac{1}{d}\right)\frac{p_\sigma}{p_\pi^2}\right]-1}. \tag{27}$$

We have neglected the p_π contribution in Eq. (26),[31] since it is second order and $p_\pi^2 \ll 1$. This is consistent with the reduced TB σ bond order being found to be almost totally independent of the choice of p_π.

The results of Eqs. (26) and (27) have important implications for the prediction of structural stability. It follows that for the three-dimensional systems diamond, simple cubic, and fcc,

$$\Theta_\sigma^{(1/2)}(2\text{hop}) = 1.96/\sqrt{z},$$

$$\Theta_\pi^{(1/2)}(2\text{hop}) \approx 0.24/\sqrt{z}, \tag{28}$$

where the constraint prefactors depend on our choice $p_\sigma=2/3$, $p_\pi=1/6$. These functions are plotted in Fig. 4 as the dashed and dotted curves, respectively, providing upper bounds to the TB values.We see that the diamond structure with $z=4$ has a saturated σ bond with a bond order of 0.98 but largely unsaturated π bonds with bond orders of 0.12. On the other hand, close-packed fcc with $z=12$ has a relatively unsaturated σ bond with a bond order of 0.56 and very unsaturated π bond orders of 0.07. This is consistent with the well-known chemistry of these three-dimensional structure types. Unfortunately, however, the conclusion that the σ and π bond orders vary inversely as the square root of the coordination implies from Eq. (14) that they display *identical* cohesive energies for the realistic case of $\lambda=2$. This supports the conclusion of Cressoni and Pettifor[15] that the structural trend across the *sp*-valent elements is driven by moments beyond the second, in particular the third and the fourth which measure the skewing and uni- versus bi-modal behavior of the DOS.

IV. EXPRESSION FOR GENERAL BOND OCCUPANCIES

A. Extrapolation of the bond order

The bond occupancies and bond orders corresponding to filling either one, two, or three poles are given directly by analytic BOP theory.[26,41] This allows, for example, the prediction of the dependence of the bond orders with occupancy that agrees exactly with the TB solution for the case of four-atom *s*-valent systems.[41] However, since the expressions for $f \neq 1/2$ are more cumbersome than for $f=1/2$, we have chosen to extrapolate our analytic expression for half-full bond occupancy to any general occupancy by using the upper-bound envelope function from Sec. III A as a boundary condition. This provides a transparent framework for performing molecular dynamics simulations of heterovalent multicomponent systems such as GaAs.[29]

We first consider the symmetric situation before we generalize the expressions to include asymmetry. We assume that the symmetric bond order $\Theta_s(f)$ is well approximated by a third-order polynomial in the symmetric function $f(1-f)$, namely,

$$\Theta_s(f) = a_s f(1-f)\{1 - b_s f(1-f)[1 - c_s f(1-f)]\}, \tag{29}$$

where the coefficients a_s, b_s, and c_s are found by satisfying the boundary conditions

$$\Theta_s(f=1/2) = \Theta_0, \quad \Theta_s'(f=1/2) = 0,$$

$$\Theta_s(f=0) = 0, \quad \Theta_s'(f=0) = 2, \quad \Theta_s''(f=0) = 0,$$

$$\Theta_s(f=1) = 0, \quad \Theta_s'(f=1) = -2, \quad \Theta_s''(f=1) = 0. \tag{30}$$

For $\Theta_0 \leqslant \Theta_s^c = 5/8$ we find that $a_s=2$, $b_s=-1$, and $c_s = 32(\Theta_s^c - \Theta_0)$. The left and central panels of Fig. 5 illustrate the behaviour of this function for $\Theta_0=1/8$ and $\Theta_0=\Theta_s^c = 5/8$, respectively. For the critical value of $\Theta_s^c=5/8$, the coefficient c_s vanishes and the polynomial becomes second order in $f(1-f)$.

For $\Theta_0 > \Theta_s^c$, we assume that the bond order merges with the envelope function Eq. (18), at some value of fractional occupancy $f_0 \neq 0$ and $(1-f_0) \neq 1$ as illustrated for $\Theta_0=7/8$ in the right hand panel of Fig. 5. This behavior is supported by

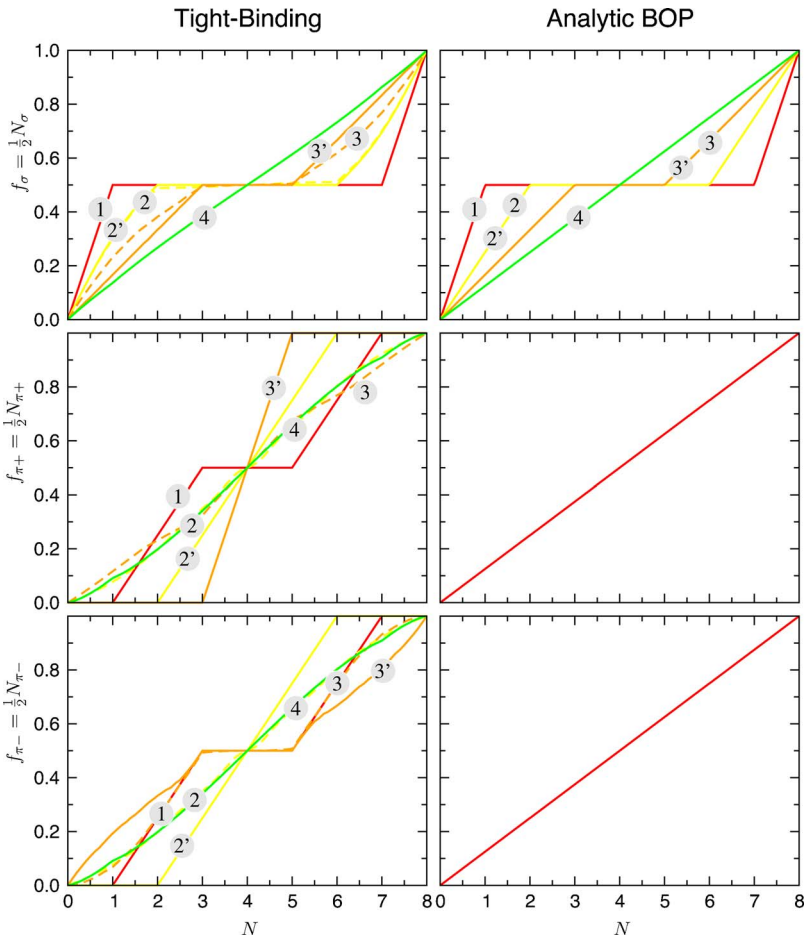

FIG. 6. (Color online) Number of electrons in the σ, π_+, and π_- bonds as a function of the total number of electrons per atom N for the case $p_\sigma = 2/3$, $p_\pi = 1/6$. Shown are the dimer (1), linear chain (2′), helical chain (2, dashed line), graphene sheet (3′), puckered graphene sheet (3, dashed line), and cubic diamond (4). The fractional occupancies in the structures with more than $z=4$ neighbors are similar to those for diamond and are not plotted here for clarity. The BOP results in the right column correspond to the bond occupations discussed in Sec. IV B.

the reduced TB results in Fig. 3 where we see that bond orders of structures with highly saturated bonds join the envelope functions smoothly before either empty or full occupancy has been reached. The analytic expression in this case can be written down immediately by rescaling the shaded areas shown in the middle panel for $\Theta_0 = \Theta_s^c$ to the new shaded area for $\Theta_0 > \Theta_s^c$ shown in the right-hand panel. This requires that the vertical height must be reduced by the scaling factor $(\Theta_0 - 2f_0)/\Theta_s^c$. Scaling the horizontal width by the same amount implies that $(1-2f_0) = (\Theta_0 - 2f_0)/\Theta_s^c$. This latter equation defines the point of matching of the bond order to the envelope function, namely,

$$f_0 = \frac{1}{2}\left(\frac{\Theta_0 - \Theta_s^c}{1 - \Theta_s^c}\right) \quad \text{for } \Theta_0 \geq \Theta_s^c. \tag{31}$$

This checks for the two cases $\Theta_0 = \Theta_s^c$ and 1 since then $f_0 = 0$ and $1/2$, respectively. For $\Theta_0 < \Theta_s^c$, f_0 vanishes by construction.

The extrapolation formula for the bond order can, therefore, be written in the general form for all values of Θ_0 as

$$\Theta_s(f) = \begin{cases} 2f & \text{for } 0 \leq f < f_0, \\ 2f_0 + a_s F[1 - b_s F(1 - c_s F)](1 - 2f_0) & \text{for } f_0 \leq f < (1 - f_0), \\ 2(1 - f) & \text{for } (1 - f_0) < f \leq 1, \end{cases} \tag{32}$$

where

$$F = [f(1-f) - f_0(1-f_0)]/(1-2f_0)^2. \tag{33}$$

The coefficients are given by $a_s = 2$, $b_s = -1$, $c_s = 32(\Theta_s^c - \Theta_0)H(\Theta_s^c - \Theta_0)$ where H is the Heaviside step function which takes the value 0 for negative arguments but 1 for positive arguments.

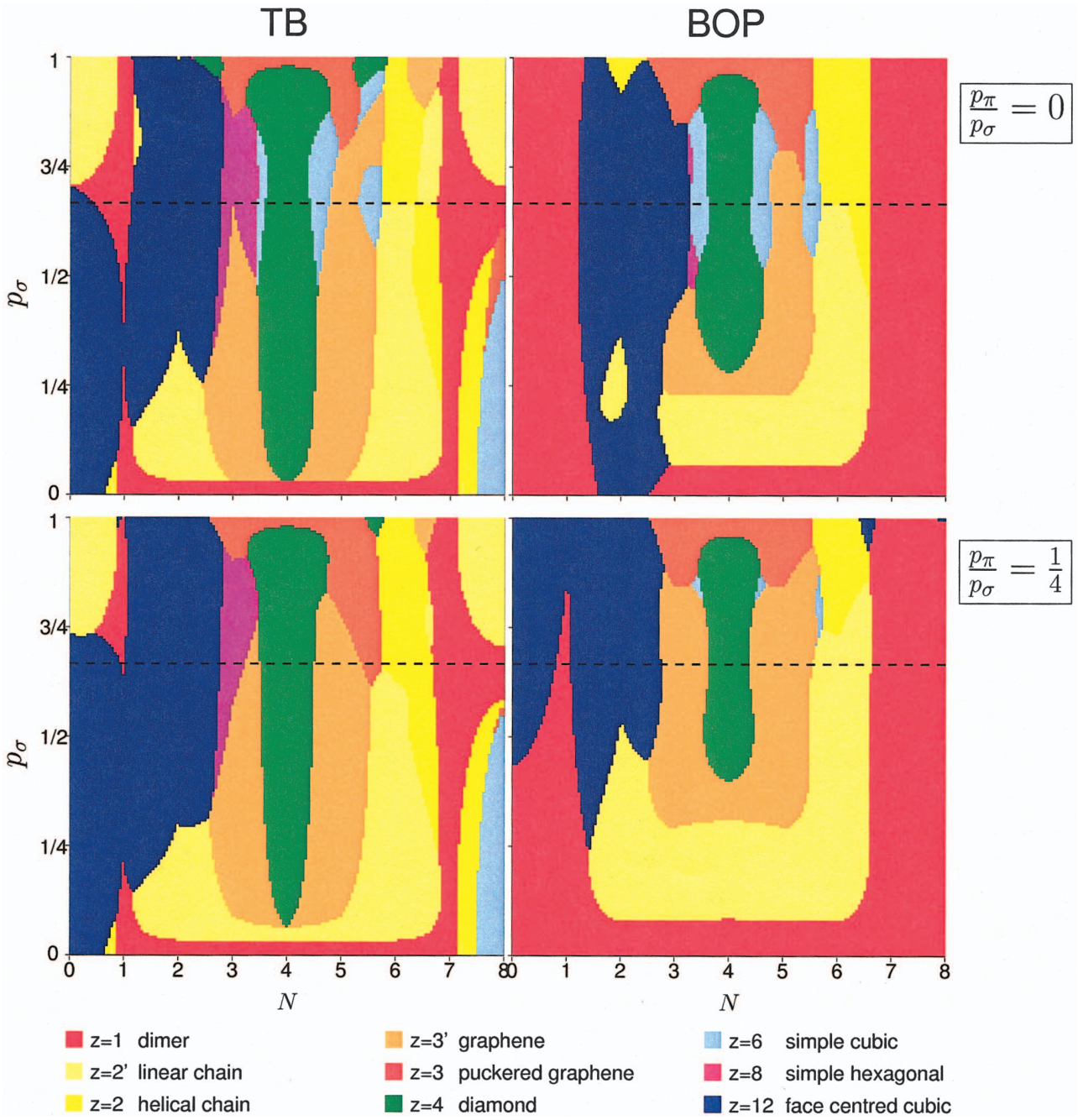

FIG. 7. (Color) Comparison of the reduced TB and analytic BOP structure maps for the case $\lambda=2$. The upper two panels correspond to $p_\pi/p_\sigma=0$; the lower two panels correspond to $p_\pi/p_\sigma=1/4$.

In Fig. 3 we see that this extrapolation, which has no free parameters, performs very well for the symmetric bond orders corresponding to $z\leqslant 6$. In particular, we find the nearly linear variation on fractional occupancy displayed by the strongly saturated σ bonds for $z\leqslant 4$ giving way to the more quadratic behavior for $z=6$. Only the cusps in some of the unsaturated π bond orders are not properly captured.

We have extended this extrapolation formula to asymmetric eigenspectra by introducing skewing into the expression, Eq. (32), by writing

$$\Theta_f = \left\{1 - k_1\left[\left(\frac{1}{2} - f\right) + k_3\left(\frac{1}{2} - f\right)^3 + k_5\left(\frac{1}{2} - f\right)^5\right]\hat{\mathfrak{R}}_3\right\}\Theta_s(f). \tag{34}$$

We have assumed that the skewing prefactor is proportional to the three-member ring contribution $\hat{\mathfrak{R}}_3$ that links the two ends of the bond. It follows from Ref. 28 that for σ bond orders this takes the form

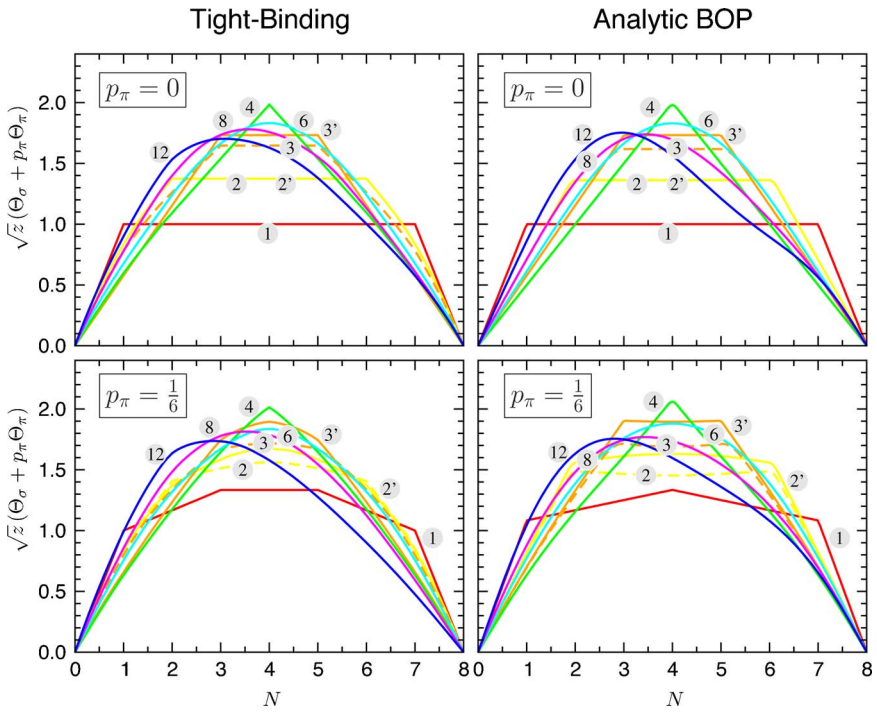

FIG. 8. (Color online) Comparison of the normalized bond orders of analytic BOP (in the right column) and the reduced TB (in the left column). The upper and lower panels correspond to $p_\sigma=2/3$, $p_\pi=0$ and $p_\sigma=2/3$, $p_\pi=1/6$, respectively. Shown are the dimer (1), the linear chain (2′), the helical chain (2, dashed line), the graphene sheet (3′), the puckered graphene sheet (3, dashed line), cubic diamond (4), simple cubic (6), simple hexagonal (8), and face-centered cubic (12).

$$\hat{\mathfrak{R}}_3^{ij} = \frac{\mathfrak{R}_{3\sigma}^{ij}}{1+\Phi_{2\sigma}} = \frac{\sum_{k\neq i,j} g_\sigma(\vartheta_i) g_\sigma(\vartheta_k) g_\sigma(\vartheta_j) \hat{\beta}_\sigma^{ik} \hat{\beta}_\sigma^{kj}}{1+\frac{1}{2}\sum_{k\neq i,j} [g_\sigma(\vartheta_i)(\hat{\beta}_\sigma^{ik})^2 + g_\sigma(\vartheta_j)(\hat{\beta}_\sigma^{kj})^2]}. \tag{35}$$

The normalized bond integrals are defined by $\hat{\beta}_\sigma^{ik} = \beta_\sigma(R_{ik})/\beta_\sigma(R_{ij})$ and the angular function depends on p_σ and the bond angle ϑ through

$$g_\sigma(\vartheta) = (1-p_\sigma) + p_\sigma \cos(\vartheta). \tag{36}$$

This skewed polynomial is made to satisfy the boundary conditions in Eq. (30) with the proviso that the first derivative of $\Theta(f)$ only matches the envelope function at either the left- or right-hand boundary depending on whether the ring contribution is negative or positive, respectively. We find that the coefficients take the values

$$a = 2/\left(1+\frac{8+k_3}{20}|k_1\hat{\mathfrak{R}}_3|\right),$$

$$b = -1,$$

$$c = \left[32+\tfrac{8}{5}(8+k_3)|k_1\hat{\mathfrak{R}}_3|\right](\Theta^c-\Theta_0)H(\Theta^c-\Theta_0),$$

$$k_5 = -\tfrac{4}{5}(4+3k_3), \tag{37}$$

where the critical bond order Θ^c takes the value

$$\Theta^c = 5\Big/\left(8+\frac{2}{5}(8+k_3)|k_1\hat{\mathfrak{R}}_3|\right). \tag{38}$$

We have fitted the two unknown parameters k_1 and k_3 to the reduced TB σ bond order for fcc in Fig. 3, finding $k_1=-3$ and $k_3=-13/6$ for $p_\sigma=2/3$ and $p_\pi=1/6$. We see that the agreement between the skewed analytic σ bond orders and the reduced TB values are good except for the bond along the c-axis in simple hexagonal. In this case there are no direct first-nearest-neighbor three-member ring terms linking the ends of the bond so that analytic BOP will be symmetric in disagreement with the positive skewing observed in TB. Nevertheless, the analytic BOP predicts the correct magnitude for half-full band occupancy. In particular, the axial bond is found to be 28% more saturated than the planar bond in good agreement with the TB value of 23%. This large difference of the bond orders is driven by the different environments about the axial and planar bonds, since the bond lengths are all identical. This will be important for the correct treatment of anisotropic structures such as α-Ga and α-As. Finally, we should note that we have not bothered to skew the π bond orders since π bonds play such a minimal role in close-packed sp-valent systems, as can be seen by comparing their σ and π bond orders in Fig. 4.

B. Relation between bond occupancy and valence electron number

We have argued in Sec. II B that the σ bonding is responsible for driving the $z=(8-N)$ rule. This is rationalized within a valence bond framework by assuming that single

saturated covalent bonds are formed with the z neighbors, thereby completing the stable octet shell of electrons about each atom as $(z+N)=8$. Within a molecular orbital or TB representation an explanation[17] is provided by introducing the hybrid orbitals sp, sp^2, or sp^3 and assuming that hybrids on different nearest-neighbor atoms do not interact unless they point toward each other. The eigenspectrum of the linear chain with $z=2$ will then have doubly degenerate sp bonding and antibonding σ states and two doubly degenerate π states (assuming $pp\pi=0$ for simplicity). The planar graphene sheet with $z=3$ will have triply degenerate sp^2 bonding and antibonding σ states and a doubly degenerate nonbonding π state. Finally, diamond with $z=4$ will have only quadruply degenerate sp^3 bonding and antibonding states. These eigenspectra are to be compared with that of the dimer with $z=1$ which has singly degenerate bonding and antibonding σ states, a doubly degenerate nonbonding σ^* state, and two doubly degenerate π states.

The origin of the $z=(8-N)$ rule can now be understood by filling these molecular orbitals of TB states with electrons, remembering that the σ bond integral and hence the strength of the bonding state decreases from the dimer through to diamond as the bond length increases with increasing coordination [cf. Eq. (14)]. Initially the dimer with $z=1$ will be most stable as it contains the deepest bonding level. However, after $N=1$ the singly degenerate bonding state is full and the nonbonding states start to occupy. This drives the structure to $z=2$, the nonbonding states start to occupy and the structure changes to $z=3$, and then after $N=3$ to $z=4$, where all four degenerate bonding states of diamond may be filled. Thus, we find the trend from $z=1\rightarrow2\rightarrow3\rightarrow4\rightarrow3\rightarrow2\rightarrow1$ as N changes from $1\rightarrow7$. The open structures for sp-valent elements with $N<4$ are not observed due to competition with close-packed or nearly close-packed structure types with their skewed eigenspectra. However, for $N\geqslant4$ we recover the $(8-N)$ rule.

This TB explanation for the $(8-N)$ rule depends sensitively on the relative occupancies of the σ and π states between different structure types. This variation is displayed in the left hand panel of Fig. 6 where the TB bond occupancies N_σ, N_{π_+}, and N_{π_-} are plotted versus the number of valence electrons N. Within the reduced TB model the σ hybrids $|i\sigma\rangle$ and $|i\sigma^*\rangle$ on atom i associated with bond ij are defined uniquely[31,32] by

$$|i\sigma\rangle = \sqrt{1-p_\sigma}|is\rangle + \sqrt{p_\sigma}|iz\rangle, \tag{39}$$

$$|i\sigma^*\rangle = \sqrt{p_\sigma}|is\rangle + \sqrt{1-p_\sigma}|iz\rangle,$$

where $|iz\rangle$ is the p orbital on atom i that points along the bond ij toward the bond center. The π bond orbitals $|i\pi_+\rangle$ and $|i\pi_-\rangle$ correspond to the two p orbitals that are normal to the bond direction along the principal axes of the 2×2 matrix representing the π bond order.[26] The occupancies for N_{σ^*} are not given in Fig. 6 since the σ^* hybrid does not contribute to the bond energy in Eq. (6) due to the appropriate bond integral between the atoms i and j vanishing. However, its value may be inferred from the sum rule

$$N_\sigma + N_{\sigma^*} + N_{\pi_+} + N_{\pi_-} = N. \tag{40}$$

The dependence of the σ bond occupancy on electron number in Fig. 6 reflects what we discussed earlier, namely, the occupancy of the bonding state saturates at $N=1$, 2, 3, and 4 for the structures with coordinations 1, 2, 3, and 4, respectively. Structures with coordination $z>4$ have not been plotted in Fig. 6 for clarity, because they essentially mirror the diagonal dependence with electron occupancy that three-dimensional diamond displays.

We will approximate this behaviour within analytic BOP theory by

$$f_\sigma = \begin{cases} \begin{cases} N/(2z) & \text{for } N \leqslant z, \\ 1/2 & \text{for } z < N < 8-z \\ 1-(8-N)/(2z) & \text{for } N \geqslant 8-z, \end{cases} & \text{when } z \leqslant 4, \\ N/8 & \text{when } z > 4. \end{cases} \tag{41}$$

The comparison with our reduced TB calculation is shown in the top right-hand panel of Fig. 6. This is an excellent approximation for all the structure types we have considered except the puckered graphene sheets, where we see a marked curvature from the linear dependence predicted by Eq. (41).

The π bond occupations in Fig. 6 are much more complicated. The dimer, linear chain, planar graphene sheet, and diamond structure all behave as expected from our simple discussion at the start of this section. However, once the linear chain and planar sheet are twisted helically and puckered, respectively, then the connection between the fractional bond occupancy f and the electron number N becomes more subtle. Since we are interested in using analytic BOPs for simulating general structural environments using molecular dynamics, we have made the simplest possible assumption that the π bond occupancies vary linearly with electron number, i.e.,

$$f_{\pi_+} = f_{\pi_-} = N/8 \tag{42}$$

for all z, as illustrated by the middle and bottom right-hand panels in Fig. 6.

This approximation to the π bond behavior could be improved by evaluating the bond occupancies and bond orders

within analytic BOP theory for $f \neq 1/2$ as has been explicitly done for four *s*-valent atom systems in Ref. 41. However, this is more complicated than using the simple approximations above. These will be applicable to general structural environments by defining the coordination z appropriately, as has been suggested, for example, by Brenner *et al.* for REBO potentials[9] and Marks for EDIP potentials.[6]

V. ANALYTIC BOP STRUCTURE MAPS

The simple expressions linking the σ and π bond occupancies to the number of valence electrons, which are given by Eqs. (41) and (42) in the last section, enable us to predict the structural energies and structure maps within the analytic BOP formalism. The right-hand panels in Fig. 2 show the structural energies for $p_\sigma = 2/3$ and $p_\pi = 0$ or 1/6, respectively. We see that the top panel for $p_\pi = 0$ reproduces very well the reduced TB curves in the left-hand panel. The main discrepancy is that the curves of the planar and puckered graphene sheets do not cross each other around $N = 5.5$. This is due to the neglect of the nonlinear dependence of the σ bond occupancy on electron number that is shown in this region of the TB curve for the puckered sheet in Fig. 6. The BOP results also reproduce well the TB curves for $p_\pi = 1/6$, although in this case the conjugated π bond contribution to the planar graphene sheet is overestimated around $N = 5$. This is due to the diagonal approximation of Eq.(42) resulting in the antibonding states of the conjugated bond not being completely filled by this occupancy (compare the BOP and TB N_{π_+} curves in the middle panel of Fig. 6).

The BOP and TB structure maps are compared in Fig. 7 for $p_\pi = 0$ in the upper panels and $p_\pi = 1/6$ in the lower panels. We see that the domains of structural stability are well reproduced by the analytic interatomic potential. In particular, the structural trend from close packed to eightfold to fourfold to threefold to twofold to onefold is clearly shown as the number of valence electrons increases from 1 to 7. Moreover, the expected favoring of the puckered threefold structure with its 90° bond angles over the planar graphitic structure is clearly observed as the relative amount of p character in the σ hybrid, p_σ, increases toward unity.

Finally, the central role played by the bond order in determining these structure maps is demonstrated by considering the dependence on the number of valence electrons of the normalized bond order $\sqrt{z}(\Theta_\sigma^z + p_\pi \Theta_\pi^z)$, where $\Theta_\pi = (\Theta_{\pi_+} + \Theta_{\pi_-})$. We know from the structural energy difference theorem and Eq. (14) with $\lambda = 2$ that the most stable structure type must display the largest value of this quantity. This is indeed the case as can be seen by comparing the resultant structural stability predictions from the TB and BOP normalized bond orders in Fig. 8 with the corresponding predictions from the structural energy curves in Fig. 2. Analytic BOP theory *predicts* the valence-driven structural trends naturally within its remit unlike all other empirical potentials which have to *refit* the relative stability of the different structure types for each particular valence.

VI. CONCLUSION

The previously published analytic BOP for group IV has been generalized to non-group-IV *sp*-valent elements. This was achieved by deriving an upper bound on the magnitude of the bond order, which allowed the value of the bond order for a half-full bond occupancy to be extrapolated to any bond filling. Simple expressions relating σ and π bond fillings to the number of valence electrons N and coordination z were obtained. These analytic BOPs were shown to predict correctly the structural trends across the *sp*-valent elements from the close-packed structures of the early groups through the diamond structure of group IV to the threefold, twofold, and onefold coordinated structures of the remaining three groups. Thus, these BOPs include the valence-dependent character of the bonding naturally within their remit unlike other empirical interatomic potentials. They are currently being extended to include ionic contributions, so that surface reconstructions and thin-film growth of heterovalent *sp*-valent systems such as GaAs may be reliably modeled.

ACKNOWLEDGMENTS

The authors acknowledge funding by DARPA/ONR under the Research Contract No. GG10551-119199. R.D. acknowledges helpful discussions with A. P. Horsfield.

[1] M. S. Daw and M. I. Baskes, Phys. Rev. B **29**, 6443 (1984).
[2] M. W. Finnis and J. E. Sinclair, Philos. Mag. A **50**, 45 (1984).
[3] S. M. Foiles, Phys. Rev. B **48**, 4287 (1993).
[4] F. H. Stillinger, and T. A. Weber, Phys. Rev. B **31**, 5262 (1985).
[5] M. Z. Bazant, E. Kaxiras, and J. F. Justo, Phys. Rev. B **56**, 8542 (1997).
[6] N. Marks, J. Phys.: Condens. Matter **14**, 2901 (2002).
[7] J. F. Justo, M. Z. Bazant, E. Kaxiras, V. V. Bulatov, and S. Yip, Phys. Rev. B **58**, 2539 (1998).
[8] J. Tersoff, Phys. Rev. Lett. **56**, 632 (1986).
[9] D. W. Brenner, O. A. Shenderova, J. A. Harrison, S. J. Stuart, B. Ni, and S. B. Sinnott, J. Phys.: Condens. Matter **14**, 783 (2002).
[10] K. Albe, K. Nordlund, J. Nord, and A. Kuronen, Phys. Rev. B **66**, 035205 (2002).
[11] A. C. T. van Duin, S. Dasgupta, F. Lorant, and W. A. Goddard III, J. Phys. Chem. A **105**, 9396 (2001).
[12] A. C. T. van Duin, A. Strachan, S. Stewman, Q. Zhang, X. Xu, and W. A. Goddard III, J. Phys. Chem. A **107**, 3803 (2003).
[13] J. Donohue, *The Structure of the Elements* (Wiley, New York, 1974).
[14] G. Allan and M. Lannoo, J. Phys. (France) **44**, 1355 (1983).
[15] J. C. Cressoni, and D. G. Pettifor, J. Phys.: Condens. Matter **3**, 495 (1991).
[16] D. G. Pettifor, J. Phys. C **19**, 285 (1986).
[17] D. G. Pettifor, *Bonding and Structure of Molecules and Solids* (Oxford University Press, Oxford, 1995).
[18] F. Cyrot-Lackmann, Adv. Phys. **16**, 393 (1967).
[19] D. G. Pettifor, Phys. Rev. Lett. **63**, 2480 (1989).

[20] M. Aoki and D. G. Pettifor, in *Physics of Transition Metals*, edited by P. M. Oppeneer, and J. Kübler (World Scientific, Singapore, 1993), p. 299.
[21] M. Aoki, Phys. Rev. Lett. **71**, 3842 (1993).
[22] D. G. Pettifor and M. Aoki, Philos. Trans. R. Soc. London, Ser. A **334**, 439 (1991).
[23] S. Znam, D. Nguyen-Manh, D. G. Pettifor, and V. Vitek, Philos. Mag. **83**, 415 (2003).
[24] M. Mrovec, D. Nguyen-Manh, D. G. Pettifor, and V. Vitek, Phys. Rev. B **69**, 094115 (2004).
[25] M. J. Cawkwell, D. Nguyen-Manh, C. Woodward, D. G. Pettifor, and V. Vitek, Science **309**, 1059 (2005).
[26] D. G. Pettifor and I. I. Oleinik, Phys. Rev. B **59**, 8487 (1999).
[27] D. G. Pettifor and I. I. Oleinik, Phys. Rev. Lett. **84**, 4124 (2000).
[28] D. G. Pettifor and I. I. Oleinik, Phys. Rev. B **65**, 172103 (2002).
[29] D. A. Murdick, X. W. Zhou, H. N. G. Wadley, R. Drautz, and D. G. Pettifor, in *Modeling of Morphological Evolution at Surfaces and Interfaces*, edited by J. Evans, C. Orme, M. Asta, and Z. Zhang, MRS Symposia Proceedings No. 859E (Materials Research Society, Warrendale, PA, 2005), JJ 9.7.
[30] R. Drautz, D. Nguyen-Manh, D. A. Murdick, X. W. Zhou, H. N. G. Wadley, and D. G. Pettifor, in *Computational Modeling and Simulation of Materials III, Part B*, Proceedings of the Third International Conference: Computational Modeling and Simulation of Materials, Acireale, Sicily, Italy, May 30–June 4, 2004 (Techna Group s.r.l., Faenza, Italy, 2005), p. 231.
[31] D. G. Pettifor, Springer Proc. Phys. **48**, 64 (1990).
[32] D. G. Pettifor, M. W. Finnis, D. Nguyen-Manh, D. A. Murdick, X. W. Zhou, and H. N. G. Wadley, Mater. Sci. Eng., A **365**, 2 (2004).
[33] J. C. Slater and G. F. Koster, Phys. Rev. **94**, 1468 (1954).
[34] W. A. Harrison, *Electronic Structure and Properties of Solids* (Freeman, San Francisco, 1980).
[35] C. H. Xu, C. Z. Wang, C. T. Chan, and K. M. Ho, J. Phys.: Condens. Matter **4**, 6047 (1992).
[36] L. Goodwin, A. J. Skinner, and D. G. Pettifor, Europhys. Lett. **9**, 701 (1989).
[37] W. B. Jensen, in *The Structure of Binary Compounds*, edited by F. R. de Boer and D. G. Pettifor, (North-Holland, Amsterdam, 1989), Chap. 2.
[38] A. P. Horsfield, A. M. Bratkovsky, M. Fearn, D. G. Pettifor, and M. Aoki, Phys. Rev. B **53**, 12694 (1996).
[39] F. Ducastelle and F. Cyrot-Lackmann, J. Phys. Chem. Solids **32**, 285 (1971).
[40] J. K. Burdett, *Chemical Bonding in Solids* (Oxford University Press, New York, 1995).
[41] D. G. Pettifor, and I. I. Oleinik, Prog. Mater. Sci. **49**, 285 (2004).
[42] M. W. Finnis, *Interatomic Forces in Condensed Matter* (Oxford University Press, Oxford, 2003).
[43] C. A. Coulson, Proc. R. Soc. London, Ser. A **169**, 413 (1939).
[44] R. Jones and M. W. Lewis, Philos. Mag. B **49**, 95 (1984).
[45] J. Inone and Y. Ohta, J. Phys. C **20**, 1947 (1987).
[46] See Eq. (3) of Ref. 28.
[47] S. R. Nishitani, P. Alinaghian, C. Hausleitner, and D. G. Pettifor, Philos. Mag. Lett. **69**, 177 (1994).